Lagrangian structures and transport in turbulent magnetized plasmas

2007 New J. Phys. 9 400

(http://iopscience.iop.org/1367-2630/9/11/400)

New Journal of Physics
The open-access journal for physics

Lagrangian structures and transport in turbulent magnetized plasmas

Kathrin Padberg[1,4], **Thilo Hauff**[2], **Frank Jenko**[2] **and Oliver Junge**[3]

[1] Institute for Traffic and Economics, Technische Universität Dresden, D-01062 Dresden, Germany
[2] Max-Planck-Institut für Plasmaphysik, Boltzmannstr 2, D-85748 Garching, Germany
[3] Faculty for Mathematics, Technische Universität München, D-85748 Garching, Germany
E-mail: padberg@vwi.tu-dresden.de, thauff@ipp.mpg.de, jenko@ipp.mpg.de and junge@ma.tum.de

New Journal of Physics **9** (2007) 400
Received 1 August 2007
Published 6 November 2007
Online at http://www.njp.org/
doi:10.1088/1367-2630/9/11/400

Abstract. Using direct numerical simulations, it is established that under realistic conditions, the turbulent transport in magnetized fusion plasmas tends to be in a regime for which the cross-field dynamics of tracers can be described neither by Eulerian nor by random walk approaches. Instead, the concept of Lagrangian coherent structures turns out to be a useful tool for studying such systems. Here, networks of repelling and attracting material lines—acting as barriers for transport—become important. The latter are analogues of the stable and unstable manifolds in the static case. This opens up new possibilities for interpreting and analyzing turbulent transport in magnetized plasmas.

[4] Author to whom any correspondence should be addressed.

PII: S1367-2630(07)56475-8

Contents

1. Introduction

Magnetized plasmas play an important role in astrophysics as well as in magnetic confinement fusion and in many other natural or technological systems. The dynamics of the plasma particles (usually electrons and one or more ion species) in such systems is highly anisotropic. While the motion along magnetic field lines is practically free (up to magnetic mirror and parallel acceleration effects), the motion perpendicular to a strong background magnetic field may be described as a superposition of a fast gyromotion and a relatively slow drift [1]. If the magnetic field is sufficiently homogeneous, i.e. drift effects due to magnetic curvature and gradients of B may be neglected, the so-called $E \times B$ drift will tend to dominate the perpendicular dynamics [1]. The underlying spatiotemporal fluctuations of the electrostatic potential are usually caused by the plasma itself. Spatial inhomogeneities in the plasma densities and/or temperatures will drive small-scale waves unstable, and the latter will then saturate nonlinearly, leading to a (statistically) quasistationary turbulent state involving many degrees of freedom. In order to distinguish the resulting transport processes from collisional ones (which are generally subdominant), they are termed 'turbulent' or 'anomalous'.

If the concentration of a given particle species is sufficiently low, the back-reaction on the turbulence may be neglected and a 'passive tracer' description is justified. This approximation makes the complex problem of turbulent transport somewhat more accessible and shall be the basis of the present study. An investigation of the relationship between test particle transport and the particle/heat transport of active species (like the electrons or the bulk ions) can be found, e.g. in [2, 3]. Our goal is to consider the $E \times B$ advection of trace ions in prescribed turbulent fields for a given perpendicular plane (see, e.g. [4] and references therein), not addressing questions related to parallel dynamics [4] and finite gyroradius effects (see, e.g. [5] and references therein). Interestingly, this problem is more or less isomorphic to the motion (with constant velocity) of charged plasmas particles along perturbed magnetic field lines—a situation which is of significant interest to both astrophysical and fusion research. Thus, while we will always speak about $E \times B$ drift-induced transport, it should be kept in mind that all of our considerations also

carry over to magnetic transport, with the parallel component of the vector potential playing the role of the electrostatic potential [4].

The turbulent fluctuations inducing the perpendicular transport may be characterized by the so-called Kubo number K which is given by the mean advection velocity normalized with respect to the ratio of the correlation length and time [6]. It turns out that this is a key dimensionless parameter in the context of tracer transport. Here, the following two limiting cases are of particular interest: very large values of K correspond to quasistatic situations in which the particles more or less follow the equipotential lines of their streamfunction, given by the electrostatic potential, and small values of K represent situations in which the particles are kicked frequently and randomly, leading to Gaussian diffusion. Now, as has been noted recently, fusion plasmas tend to exhibit Kubo numbers in the intermediate range of unity [7]. This implies that neither limiting case applies, making the turbulent transport problem especially challenging and interesting. Also, Eulerian techniques trying to connect some basic properties of the potential structures with the transport coefficients will fail in the $K \sim 1$ regime. This motivated us to explore the recently developed concept of *Lagrangian coherent structures* (LCS) (see, e.g. [8]–[11]). These structures can be seen as time-dependent analogues to invariant manifolds in dynamical systems theory and as such they naturally form a skeleton of the dynamics and particle transport. LCS can be detected and approximated using finite-time Lyapunov exponents (FTLE) or relative dispersion and related techniques. As will become clear in the course of this work, these novel concepts are very well suited to analyzing turbulent transport in magnetized plasmas.

The remainder of this paper is organized as follows. In section 2, we present the basic dynamical equations for the problem under investigation together with the ways the advection fields are computed. Moreover, the Kubo number—which is a key quantity characterizing the random/turbulent fields—is introduced. In section 3, some classical concepts from dynamical systems theory are reviewed first to motivate the recently developed approaches for time-dependent systems. In particular, the approximation of invariant manifolds and LCS via FTLE or related techniques is illustrated by a simple example. In section 4, these techniques are applied to the velocity fields introduced in section 2. More specifically, we describe and discuss the computational results for different self-created potentials as well as for realistic turbulent plasma simulations. We close this work with a brief summary and an outlook in section 5.

2. Magnetized plasmas: random and turbulent fields

Throughout this paper, we consider the $E \times B$ advection of ions as passive tracers in a plane perpendicular to the background magnetic field, where the corresponding spatial coordinates will be denoted as $\mathbf{x} = (x, y)$. The fluctuating electrostatic potentials $\Psi(\mathbf{x}, t)$ will either be taken from simulations with the plasma turbulence code GENE [12, 13]—solving the nonlinear gyrokinetic equations in three spatial and two velocity space dimensions—or they will be self-created by superposing a sufficiently large number of harmonic waves,

$$\Psi(\mathbf{x}, t) = \sum_{i=1}^{N} A_i \sin(\mathbf{k}_i \cdot \mathbf{x} + \omega_i t + \varphi_i) \,, \tag{1}$$

where the amplitudes A_i, wave vectors $\mathbf{k}_i$, frequencies ω_i and phases φ_i are chosen randomly from certain (physically motivated) distribution functions [5].

The motion of the gyrocenter of a passive particle is then described by the (normalized) $E \times B$ drift velocity according to the differential equations

$$\dot{x} = -\frac{\partial \Psi}{\partial y}(x, y, t), \qquad \dot{y} = \frac{\partial \Psi}{\partial x}(x, y, t). \tag{2}$$

We note that finite gyroradius effects are neglected here for simplicity, but could be included in a straightforward fashion [5]. It is both interesting and useful to realize that—in the language of classical mechanics—the variables x and y in equation (2) are canonically conjugated, spanning the phase space. This means that the electrostatic potential $\Psi(x, y, t)$ may also be interpreted as the Hamiltonian of a time-dependent system with one degree of freedom. Consequently, in the special case of a static potential, the problem is completely integrable. However, the introduction of a time dependence of the potential leads to chaos, which makes it necessary to use numerical methods to study the particle motion. On the other hand, one can also interpret $\Psi(x, y, t)$ as the streamfunction for the particle motion in the spirit of two-dimensional (2D) hydrodynamics. This is obvious from the relation $\dot{\mathbf{x}} \cdot \nabla \Psi = 0$ which states that the particles (gyrocenters) move tangential to $\Psi = \text{const}$ lines at any instant in time. Due to $\nabla \cdot \dot{\mathbf{x}} = 0$, the flow is incompressible. We note in passing that incompressibility does not hold exactly any more in a tokamak, since the magnetic field is not homogeneous. In the GENE simulations, compressibility effects are included, affecting the character of the turbulent potential and thus indirectly also the tracer dynamics.

The equations of motion are solved numerically via a standard fourth-order Runge–Kutta method [14]. For the self-generated potentials, the values of the potential and those of the required derivatives are given analytically for each point in space and time, whereas for the realistic, gyrokinetic potentials they are given as 3D arrays, $\Psi(x_i, y_j, t_k)$. In the latter case, the values at intermediate space-time positions are obtained by means of a suitable interpolation scheme (for details see the appendix).

A key quantity characterizing the potential fluctuations is the Kubo number [6, 15]

$$K \equiv \frac{V \tau_c}{\lambda_c} = \frac{\tau_c}{\tau_{fl}}. \tag{3}$$

Here, τ_c and λ_c denote, respectively, the autocorrelation time and length of the electrostatic potential, V is the mean drift velocity, and τ_{fl} is the mean time of flight for a distance of one correlation length. The limits $K \to \infty$ and $K \to 0$ correspond to static and fast fluctuations, respectively. Sometimes, the regime of $K \lesssim 1$ is labeled 'weak turbulence' or 'quasilinear,' while the $K \gtrsim 1$ regime is called 'strong turbulence' or 'nonlinear.' The Kubo number can be regarded as a measure for the ability of the particles to explore the structure of their streamfunction. Whereas this is possible for $K \gg 1$ ($\tau_c \gg \tau_{fl}$), in the case of $K \ll 1$ ($\tau_c \ll \tau_{fl}$), the potential structures do not persist long enough. From this point of view, it is clear that these two regimes are fundamentally different.

The scaling of the particle diffusion coefficient D with the Kubo number K has been the subject of various previous studies (see, e.g. [16]–[19]). In the limit of small Kubo numbers, $K \lesssim 1$, the diffusion coefficient is known to scale like $D \propto \lambda_c V K = \tau_c V^2$, since it corresponds to a random walk with step length $\tau_c V$ and time step τ_c. In the limit of large Kubo numbers, $K \gtrsim 1$, one has

$$D \propto \lambda_c V K^{\gamma - 1} = \lambda_c^{2-\gamma} V^{\gamma} / \tau_c^{1-\gamma}, \tag{4}$$

with $\gamma < 1$ (due to trapping effects) [18, 19]. In [16] (see also the review article [17]), a consideration based on percolation theory suggests $\gamma = 0.7$ for isotropic turbulence—a result

which has been confirmed by direct numerical simulations [18, 19]. Since this consideration is based on weakly time-dependent potentials, it is valid only for large Kubo numbers. We note in passing that the small Kubo number result can also be expressed in the form of equation (4), setting $\gamma = 2$.

As has been already noted in the introduction, gyrokinetic simulations show that turbulent magnetized fusion plasmas tend to exhibit Kubo numbers in the range of unity, i.e. in the transitional regime. This makes the analysis particularly interesting but also challenging. As it will turn out, a helpful tool in this context is the notion of LCS which will be introduced and discussed next.

3. Invariant manifolds and Lagrangian coherent structures

The particle motion analyzed in the present work is described by a nonautonomous differential equation

$$\dot{\mathbf{x}} = f(\mathbf{x}, t), \tag{5}$$

where $\mathbf{x} \in \mathbb{R}^2$ denotes the position of the particle. More specifically, we consider incompressible flows which obey equation (2). For this set-up, the respective system admits a streamfunction (or electrostatic potential) $\Psi(x, y, t)$.

In case this potential does not explicitly depend on time, the motion of passive tracers is completely determined by level sets of Ψ. Moreover, the stable and unstable manifolds of hyperbolic equilibria form separatrices between invariant sets and thus serve as natural barriers to particle transport. Time-dependent analogues to these invariant manifolds continue to govern transport in nonautonomous systems. Here, statistical concepts such as FTLE or relative dispersion are used to pinpoint the geometric structures of interest.

The application of such dynamical systems ideas to study the flow geometry and hence, the mechanism to passive particle transport in nonautonomous systems has been studied in a variety of settings, see, e.g. [8]–[11], [20]–[23]. Different applications of these concepts and techniques, in particular for the analysis of fluid flows, can be found, e.g. in [24]–[30].

In the remainder of this section, a simple example is used to illustrate the geometrical concept of invariant manifolds and their counterparts in the time-dependent case, LCS, and relate it to the statistical concept of FTLE. The section closes with a short description of the numerical methods used for the approximation of barriers to transport.

3.1. Invariant manifolds

As a simple example we consider the streamfunction

$$\Psi(x, y, t) = \tfrac{1}{2}x^2 - \tfrac{1}{4}x^4 - \tfrac{1}{2}y^2 - \varepsilon x \cos(t), \tag{6}$$

and obtain the time-periodic ordinary differential equation

$$\dot{x} = y\,, \quad \dot{y} = x - x^3 - \varepsilon \cos(t)\,. \tag{7}$$

This system corresponds to the periodically forced Duffing oscillator without friction (i.e. the conservative Duffing system; see, e.g. [31] for a detailed discussion of this model). We first consider the case $\varepsilon = 0$, which is the autonomous (time-independent) situation. The system admits three equilibria—an unstable fixed point at the origin and two (marginally) stable stationary solutions at $(x, y) = (\pm 1, 0)$. Since the origin is a hyperbolic saddle point,

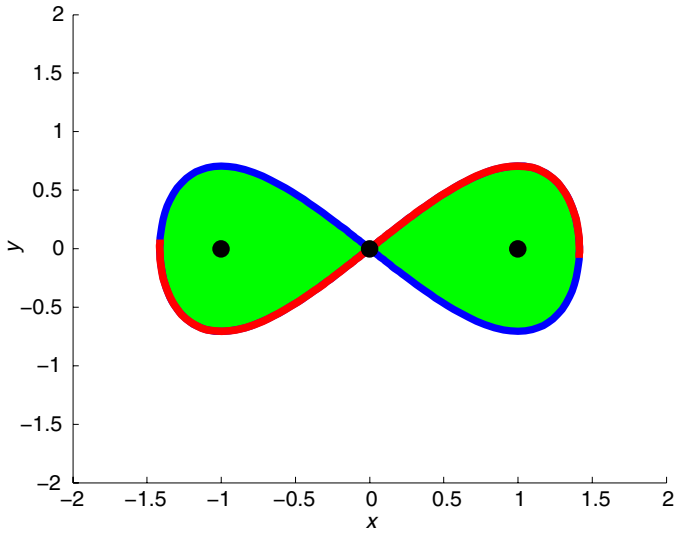

Figure 1. Equilibria (black), global stable (blue) and unstable (red) manifold of the origin in the conservative Duffing oscillator.

the existence of stable and unstable manifolds is guaranteed (i.e. the sets of those initial conditions that evolve asymptotically towards the equilibrium in forward and in backward time, respectively). See, e.g. [31] for a thorough introduction to these classical concepts from dynamical systems theory.

The global stable and unstable manifolds of the origin look like shown in figure 1. In fact, in this case these two manifolds coincide and form so-called homoclinic orbits. These two orbits separate phase space into three invariant sets (i.e. sets which a trajectory of the system cannot leave in forward or in backward time): the two sets surrounding the two equilibria $(\pm 1, 0)$ (green in figure 1, left), as well as the set outside the two 'homoclinic loops' (white in figure 1). More generally, if the unstable manifold of some equilibrium coincides with the stable manifold of a different one, one speaks of a heteroclinic orbit. Again, depending on the particular geometry of the equilibria and their invariant manifolds, different heteroclinic orbits may partition phase space into invariant sets. As we will see in section 4, certain transport phenomena in a turbulent plasma can be explained by the formation (and persistence) of invariant or nearly invariant sets bounded by homoclinic or heteroclinic structures.

Stable and unstable manifolds often can also be characterized from a variational point of view: consider the flow map $\varphi_t^{t+T} : \mathbf{x}(t) \to \mathbf{x}(t+T)$ which maps fluid particles from an initial position $\mathbf{x} \in \mathbb{R}^2$ at time t to their location at time $t+T$. The FTLE with respect to $\mathbf{x}$ and t and T is then defined as

$$\sigma_t^{t+T}(\mathbf{x}) = \frac{1}{|T|} \log \left\| \frac{\mathrm{d}\varphi_t^{t+T}(\mathbf{x})}{\mathrm{d}\mathbf{x}} \right\|, \tag{8}$$

where $\|\cdot\|$ denotes the spectral norm. This quantity measures the maximum exponential growth of infinitesimal perturbations in the initial condition $\mathbf{x}$ under the (linearized) flow. It is thus a measure for how much (at most) two points in a small neighborhood of $\mathbf{x}$ get separated by the flow over the time span $[t, t+T]$. The FTLE field (i.e. with respect to initial conditions on a grid) computed in forward time in our example system takes particularly high values on the stable manifold of the origin, see figure 2(a). This is due to the fact that two points

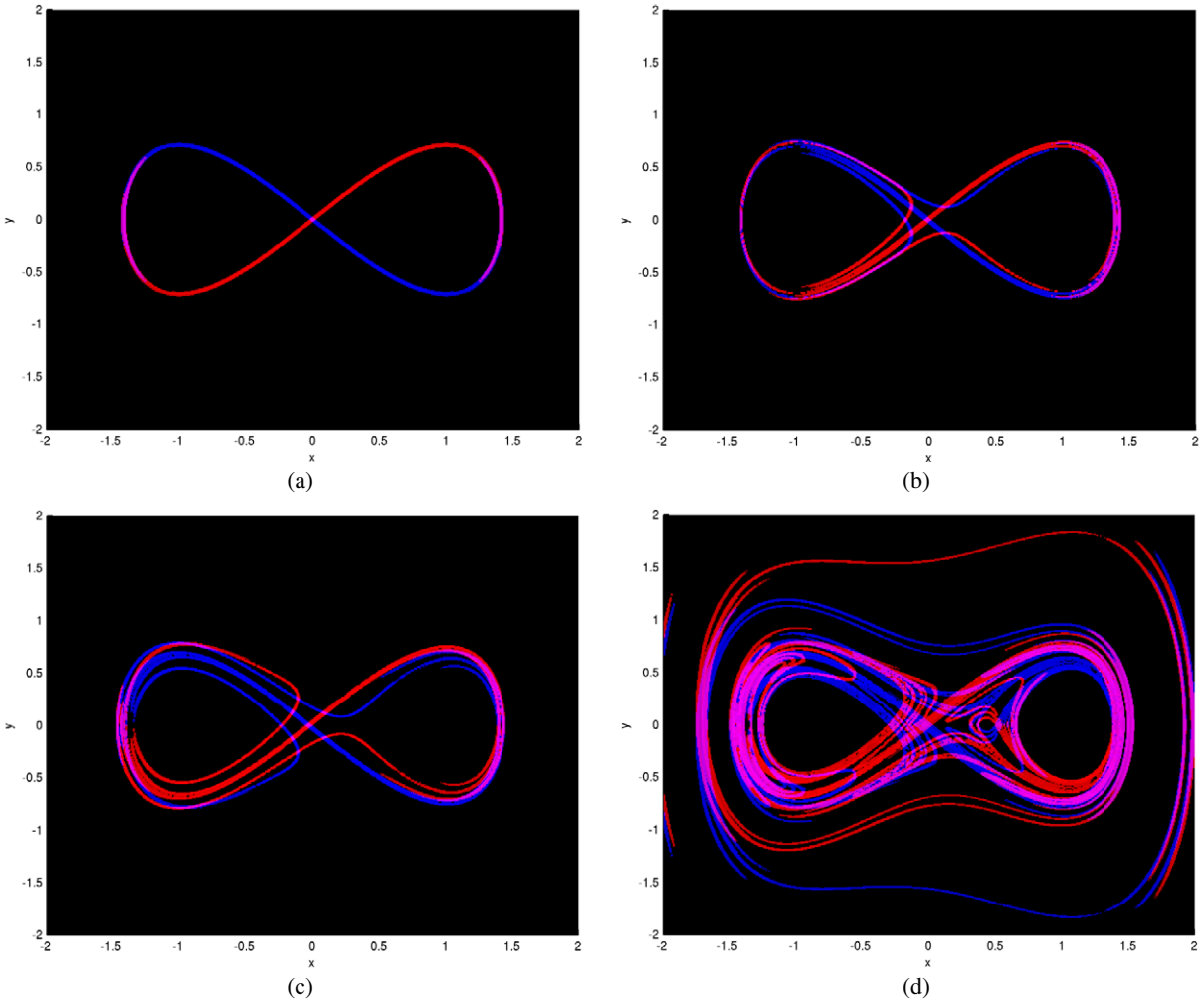

Figure 2. Regions with large values of FTLE approximate parts of the stable (blue) and unstable (red) manifold of the origin in the conservative, periodically perturbed Duffing oscillator for different choices of parameters in equations (7) and (8). (a) Autonomous Duffing oscillator ($\varepsilon = 0$ and $T = \pm 2\pi$). (b) Small periodic forcing ($\varepsilon = 0.02, t = 0\ T = \pm 4\pi$). (c) Increasing the forcing ($\varepsilon = 0.05$, $t = 0$ and $T = \pm 4\pi$). (d) Doubling the integration time ($T = \pm 8\pi$), larger portions of the manifolds are picked up ($\varepsilon = 0.05$ and $t = 0$).

straddling the manifold typically separate exponentially fast when approaching the fixed point. Such divergent behavior distinguishes them from other arbitrary particle pairs; likewise for the unstable manifold when the system is considered under time reversal. For a more detailed discussion see, e.g. [23].

Let us now consider the case of a small but finite ε in our example. This yields a time-periodic system of period 2π. If one reduces the analysis to the time 2π-flow map, the origin is a hyperbolic fixed point of the resulting time-discrete system (and hence part of a hyperbolic periodic orbit for the full system). However, now the homoclinic connection is broken with the invariant manifolds intersecting transversally and allowing for horseshoe dynamics. Using the

same arguments as above, the stable and unstable manifolds can be pinpointed using FTLE; see figure 2 for different choices of ε and T. The interior of the homoclinic loops is no longer invariant but transport is possible via the homoclinic tangles. This mechanism is called lobe dynamics; see, e.g. [32] for details.

3.2. Lagrangian coherent structures

Analytical conditions for the existence of finite-time hyperbolic manifolds in aperiodic flows have been derived, e.g. in [8]–[10], [21]. These time-dependent structures play an analogous role to the invariant manifolds that we have illustrated above and they are referred to as LCS. As has been noted in these publications, the derived analytical criteria have a strong correspondence to extrema of the FTLE fields. This notion has been analyzed in [11] where LCS are defined as ridges in the scalar FTLE field. There, an analytical formula for the flux across these structures is derived and shown to be close to zero. In this sense, LCS can indeed be seen as time-dependent analogues of stable and unstable manifolds in autonomous systems.

Therefore, the concepts described above carry over to the setting of aperiodic time dependencies: local maxima or ridges in the FTLE field correspond to *repelling material lines* (i.e. finite-time stable manifolds), and using the FTLE field of the time-reversed system, *attracting material lines* (i.e. finite-time unstable manifolds) can be obtained. These structures define natural barriers to transport, and the transport mechanism between the regions obtained can be again explained in terms of lobe dynamics via the transversal intersection of these material lines.

3.3. Numerical computation of FTLE

In principle, FTLE can be obtained by solving equation (8) for initial particles on a grid. As in most cases of practical interest, an analytical description of the total derivative of the right-hand side of the underlying differential equations is not available (typically, the velocity field is only given in the form of discrete data), forcing us to use a finite approximation of this infinitesimal quantity. For our computations, we consider a fine-meshed regular $m \times m$-grid (where m typically equals 256 or 512) and seed initial particles on this grid. We integrate the Lagrangian dynamics of each tracer, as well as the particles on the eight neighboring grid points. After time T, we calculate the relative maximum square distance of the central particle to the satellite particles:

$$\delta_t^{t+T}(x) := \frac{1}{|T|} \log \left(\max_j \frac{\|\varphi_t^{t+T}(x) - \varphi_t^{t+T}(n_j(x))\|}{\|x - n_j(x)\|} \right), \tag{9}$$

where x denotes the central particle and $n_j(x)$, $j = 1, \ldots, 8$ the neighboring grid points. This idea is very much in spirit of the relative dispersion approaches (as discussed, e.g. in [25, 33, 34]) which use finite initial perturbations for an approximation of FTLE. Since almost all initial perturbations will align along the direction of maximum growth, the quantity $\delta_t^{t+T}(x)$ will be a reasonable approximation of $\sigma_t^{t+T}(x)$ for fine enough grids. See [23] for a detailed discussion of this approach as well as related ones.

We note that our techniques are used to numerically study LCS and understand the mechanism of particle transport in realistic turbulent plasma simulations. Additional criteria for the extraction of these finite-time objects can be found e.g. in [11, 21, 30].

4. Lagrangian and Eulerian structures in turbulent plasmas

As pointed out above, the study of LCS is expected to provide new insight into the mechanisms of turbulent transport at intermediate Kubo numbers ($K \sim 1$) like they are found in first-principles simulations of plasma turbulence [7]. This is because in that transitional regime, neither a pure random walk approach ($K \ll 1$) nor a Eulerian perturbation approach ($K \gg 1$) is valid. The latter assumes that the time variations are relatively slow such that the particles still more or less follow the equipotential lines ($\Psi = \text{const}$). However, for $K \sim 1$, the autocorrelation time of the potential is roughly the same as the time required for the particles to cross a typical structure size. Thus, while the particles 'feel' the turbulent structures, they change so rapidly that the web of equipotential lines is no longer a good indicator for the characteristics of the particle motion. In the present section, we will show and discuss a series of movies which will illustrate these points, first using self-created random potentials, then employing realistic simulation data obtained from first-principles plasma turbulence simulations.

All results are obtained via approximating the quantities $\delta_t^{t+T}(x)$ in equation (9) for different initial times t and initial particles on a dense grid. The computational set-up for these simulations is described in the appendix.

4.1. Lagrangian and Eulerian structures in random fields

Let us first address the case of self-created random potentials—a mock-up of real turbulence data. The main advantage of using such an approach is that several complications (as discussed, e.g. in [7]) occurring in more realistic situations are absent, and that the key parameters (first and foremost, the Kubo number) are easier to control. Figures 3–5 display the chaotic motion of sets of test particles as induced by the $E \times B$ drift velocity in such random potentials. It is instructive to view each of these movies several times, concentrating on different particles and trying to identify interesting modes of motion. For comparison, the equipotential lines of Ψ (white structures) and the LCS (red and blue lines as previously explained) are plotted as well—the former representing the Eulerian, the latter the Lagrangian description.

Figure 3 shows the extreme case of a static streamfunction $\Psi(x, y)$, corresponding to $K = \infty$. As can be seen in the animation, the particles simply move deterministically along the equipotential lines of the streamfunction as required by the equations of motion, equation (2). The stable and unstable manifolds tend to lie near the lines described by $\Psi \approx 0$, separating the potential hills from the valleys, and therefore the invariant sets from each other. The crossing points of the homoclinic loops formed by parts of the LCS coincide with the hyperbolic saddle points of the potential landscape. Typically, particles approaching a saddle point first follow the stable manifold (blue) which is repulsive and are then attracted by an unstable manifold (red). This case may serve as a reference point for the cases with time dependence, i.e. finite Kubo number.

In a first step, we reduce the Kubo number down to $K = 5$. The corresponding results are shown in figure 4. In this animation, we observe that the particles still largely follow the equipotential lines. Moreover, the latter more or less coincide with the LCS. However, it can already be seen that the LCS are able to predict the motion of the particles for a longer time. For example, the Lagrangian analogues to hyperbolic fixed points (i.e. hyperbolic trajectories at the crossings of attracting and repelling LCS) occur long before an instantaneous saddle point in the Eulerian potential field is created. In that sense, the study of the LCS leads to a better

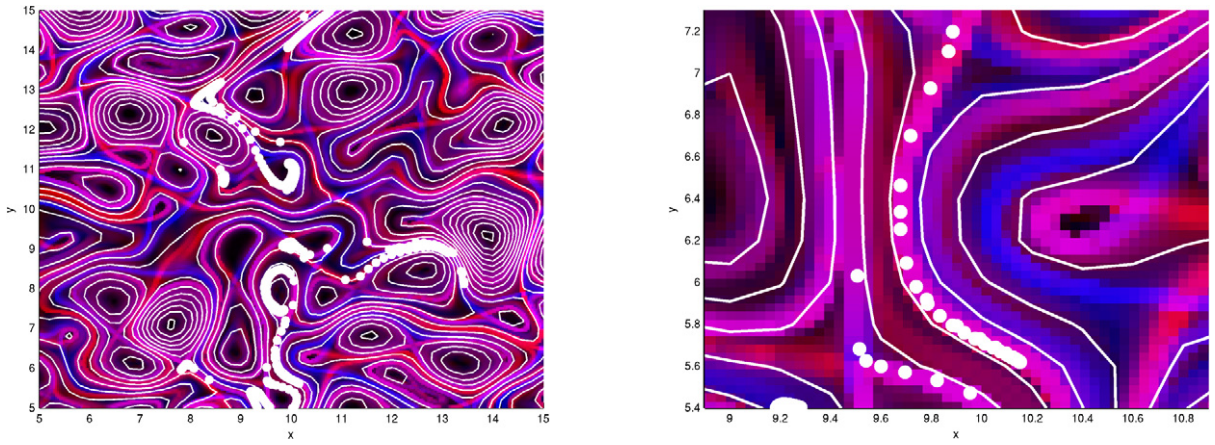

Figure 3. Simulation results for self-created static potential ($K = \infty$). Here, the equipotential lines (white) coincide with the LCS obtained via the integration of particle trajectories. In addition, the repelling (blue) and attracting material lines (red) correspond to stable and unstable manifolds of hyperbolic fixed points. (a) The animation (statpot.avi, 2.7 MB) shows how the motion of test particles is determined by these objects. In particular, particles are attracted towards hyperbolic fixed points along stable manifolds and then repelled along the different parts of the unstable manifolds. (b) Zoom on a set of particles that have aligned along the unstable manifold (i.e. attracting LCS) of a hyperbolic fixed point.

description of the particle motion than the study of the streamfunction. The differences become even more apparent as the Kubo number is lowered further.

A representative example for $K = 1.25$ is displayed in figure 5. One notes significant differences with respect to the previous case. The LCS are now practically independent of the equilines of the streamfunction, and, in general, the particles do not follow the latter any more. On the other hand, the notion of repelling and attracting material lines acting as transport barriers becomes important (see section 3), analogously to the stable and unstable manifolds in the static case. As was said before, a Kubo number in the range of unity means that the correlation time τ_c of the potential structures is comparable to the average time of flight τ_{fl} of a particle across such structures. This means that the structures (the Eulerian ones, as well as the Lagrangian ones) do not exist long enough for the particles to really explore them. In the Eulerian picture, this means that predictions about the particle motion are not possible any more by studying the potential structure, since, as can be observed in the animation, equipotential lines may move rapidly without affecting the particles. In contrast, the LCS act as transport barriers. Although their time variation seems to be slower than the variation of the streamfunction (which is due to the fact that they are calculated based on the particle motion), they take the particles with them as long as they persist. So the particle motion is restricted—and to a large degree even governed—by the motion of the LCS and the dynamic regions enclosed by those material lines.

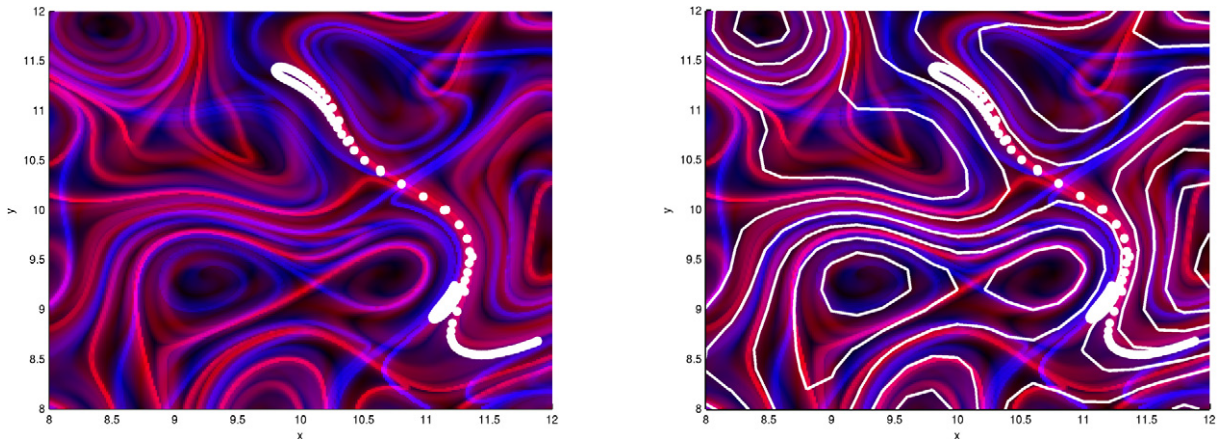

Figure 4. Simulation results for self-created random potential, Kubo number $K = 5$. (a) In the animation (kubo5.avi, 1.6 MB) one observes how the motion of particles is determined by the repelling (blue) and attracting LCS (red). Hyperbolic trajectories continue to play the role of their steady counterparts. Here, a line of particles is repelled from the hyperbolic trajectory along different parts of the attracting LCS. (b) Same animation as in (a) but with equipotential lines superimposed (kubo5pot.avi, 2.6 MB). The Lagrangian structures can predict the particle motion more accurately than the Eulerian, although—because of the slow fluctuation—the two notions are still very much related.

4.2. Lagrangian and Eulerian structures in realistic turbulent fields

Of course, the self-created random potentials used so far can only be viewed as a proxy for more realistic plasma turbulence data. In the fusion community, it is widely accepted that ab initio simulations of turbulence in the core of fusion experiments are to be based on the nonlinear gyrokinetic equations as first derived in the 1980s [35]–[37]. Here, the fast gyromotion can be removed (decoupled) from the basic equations analytically, leading to a system of partial integro-differential equations for the distribution functions of the particles in 5D phase space (three spatial coordinates—describing the position of the gyrocenters—and two velocity space coordinates) plus time. These equations are then solved numerically on massively parallel computers. In the present case, we used the gyrokinetic turbulence code GENE [12, 13] which is one of the state-of-the-art tools in the field.

It should also be pointed out that it is not possible to obtain a universal description of plasma turbulence since its character largely depends on the microinstabilities that drive it [38]. Density and/or temperature gradients in the plasma destabilize small-scale waves, and the latter will then saturate nonlinearly, leading to a (statistically) quasistationary turbulent state involving many degrees of freedom. In that nonlinear state which is far from thermodynamic equilibrium, various linear features can persist, however, as is observed in the gyrokinetic simulations [12, 13]. For our present study, we focus on turbulence driven by so-called trapped electron modes. Some of the key features of this kind of plasma turbulence is described in [13]. We take the standard parameters quoted therein, and restrict to the data in a perpendicular plane on the low-field side of a toroidal fusion device (the 'outboard midplane').

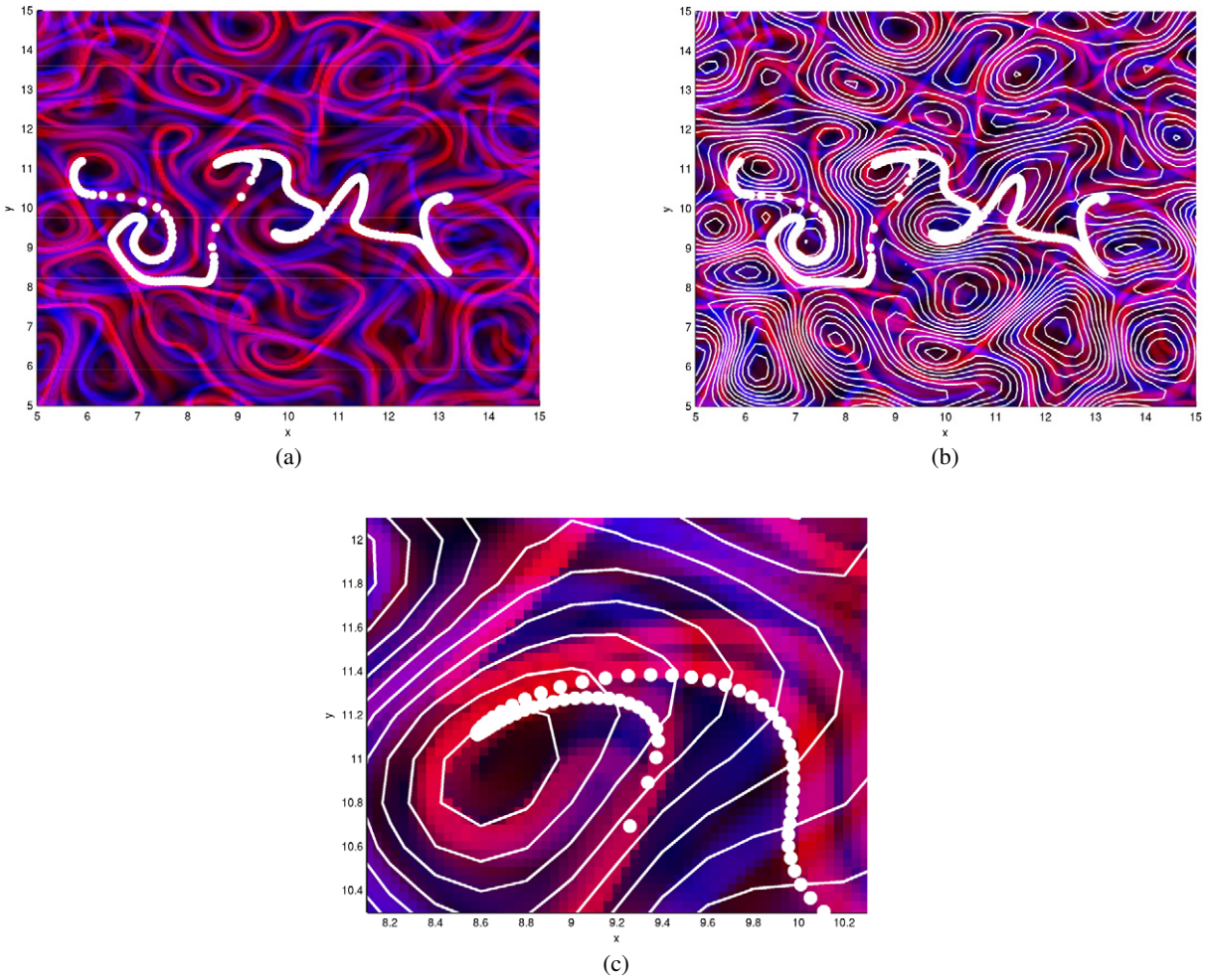

Figure 5. Simulation results for self-created random potential, $K = 1.25$. (a) In the animation (kubo125.avi, 2.8 MB) the motion of passive particles and their interaction with LCS can be observed. (b) Equipotential lines superimposed on the LCS field are used to demonstrate the differences between Eulerian and Lagrangian quantities and the importance of the latter for particle motion (kubo125pot.avi, 5.4 MB). (c) Zoom on a set of particles confirms their alignment along attracting material lines (red) and the loss of the Eulerian influence on particle motion.

The dynamics of the tracers in such realistic turbulence data is shown in figure 6. Here, the electrostatic potential in that particular plane is written out frequently during the simulation and then subjected to post-processing as outlined in section 2. The trapped electron mode potential is not isotropic any more but exhibits streamers in the radial x-direction, increasing the particle motion with respect to the y-direction. The Kubo number can be calculated to be $K \approx 2$–3, which is somewhere between the examples given in figures 4 and 5. Like one might have expected, the motion of the tracers along the repelling and attracting material lines can be observed. Moreover, frequently particles get 'trapped' in dynamic regions enclosed by LCS and are advected by the motion of these sets. Another observation is that free particles

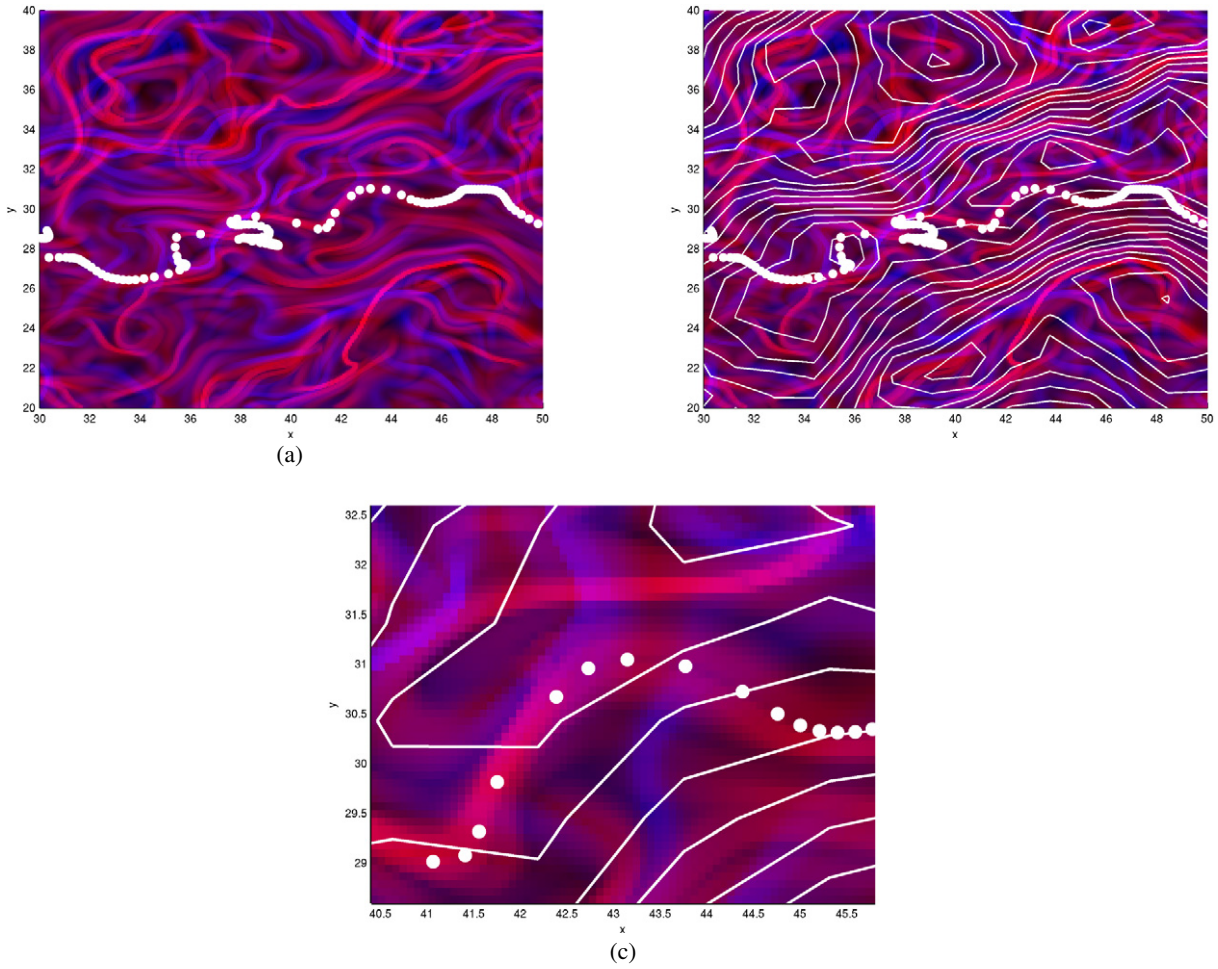

Figure 6. Plasma turbulence simulation. (a) The animation (plasma.avi, 3.3 MB) shows the motion of passive particles and their interaction with LCS. In particular, one can observe fast moving free particles, as well as trapping phenomena. (b) The animation of LCS with equipotential lines superimposed (plasmapot.avi, 4.3 MB) demonstrates the differences between Eulerian and Lagrangian quantities: LCS are more persistent and influence particle motion to a much larger degree than the equipotential lines. (c) Zoom on a set of particles confirms their alignment along attracting LCS (red) and the loss of Eulerian influence on particle motion.

typically move much faster than the LCS. However, when trapped, their velocity and motion is determined by the slower LCS advection. In addition, the approximated Lagrangian structures tend to be more persistent than the Eulerian structures, i.e. they live longer. This behavior can be interpreted as some sort of dynamical trapping—which is different from trapping in potential wells. One also observes that the LCS fields give a much more fine-scaled picture of the dynamics than the potential landscapes. For instance, invariant sets defined as the interior of heteroclinic connections in the instantaneous velocity field have a diameter of up to 10–12 gyroradii, see figure6(b). At the same time, regions enclosed by LCS typically have a size of 2–5 gyroradii. Thus, despite the fact that this data set contains several additional effects

(like poloidal drifts and others discussed in [7]), it still has many things in common with the case for $K = 1.25$ shown and discussed above.

5. Summary and outlook

The main purpose of the present work has been to establish that the concept of Lagrangian coherent structures is a useful tool for studying the transport of tracers in turbulent fusion plasmas. As it turns out, first-principles (gyrokinetic) simulations of plasma turbulence show that Kubo numbers of the order of unity are to be expected, and in this intermediate regime neither a pure random walk approach (valid for $K \ll 1$) nor Eulerian approaches (valid for $K \gg 1$ and working with snapshots of the velocity field) are adequate. Under these conditions, the particles do not follow the equilines of the streamfunction any more. On the other hand, the notion of repelling and attracting material lines acting as transport barriers becomes important. The latter are analogues of the stable and unstable manifolds in the static case. We found that Lagrangian structures tend to be smaller and more persistent than the Eulerian structures, and that the particle motion is restricted—and to a large degree even governed—by the motion of the LCS and the dynamic regions enclosed by them. This opens up new possibilities for interpreting and analyzing turbulent transport in magnetized plasmas.

The quantification of transport in these systems, i.e. the estimation of probabilities of particle transport between different regions of interest, will be subject to future studies. The computation of transport in terms of lobe dynamics has received considerable scientific interest in the last few years, see, e.g. [24, 28, 32]. Heteroclinic tangles formed by intersections of repelling and attracting LCS may explain the microscopic transport mechanism between free particles and regions enclosed by LCS. Transport probabilities can be obtained by an estimation of the volumes. However, apart from computational difficulties due to the often coarse resolution of the data, transport estimations in turbulent flows and at a macroscopic scale are not feasible by these methods. Here, transfer operator techniques such as described in [23] have a number of advantages because they do not rely on specific dynamics and transport mechanisms. Recent work on this concept also includes the detection of macroscopic structures in time-dependent systems that are maximally isolated in terms of inter-particle transport [39]. These approaches will be used to further investigate transport in turbulent magnetized plasmas.

Acknowledgments

The research of K P has been partially supported by a Research Grant of the University of Paderborn and the DFG Research Training Group GK-693 of the Paderborn Institute for Scientific Computation (PaSCo).

Appendix

In this appendix, we briefly discuss some technical details of our computations: in all cases, we consider test particles on a 256×256 grid. The trajectories are integrated by means of a fourth-order Runge–Kutta scheme. The velocities are obtained via cubic interpolation in space, as well as linear interpolation in time with respect to the underlying data grid. The integration time span of the particle trajectories has been chosen according to the characteristics of the specific

system under consideration. Typically, the longer the time span, the more structures are picked up, often resulting in a very detailed picture where dominant structures are no longer discernible. To determine an appropriate integration time, one usually relies on numerical experiments, as well as on the application of scaling laws from turbulence studies (see, e.g. [23] and references therein).

A.1 Artificial potentials

The artificial potentials are provided on spatial grids $[0,\ 20]^2$, with meshsize $\Delta x = \Delta y = 0.2$ and the time resolution of data set is $\Delta\tau = 5$, resulting in $200 \times 200 \times 201$ data arrays. For the integration of the particle trajectories, we choose a step size of $h = 0.1$ in the Runge–Kutta scheme. The movies are presented at a time resolution of $\Delta\hat{\tau} = 1$, i.e. the time distance between two movie frames. For the special case of data for Kubo number $K = 5$, we seed initial particles on the grid $[8,\ 12]^2$ with meshsize 0.016 at initial times $n\Delta\hat{\tau}$; $n = 0, \ldots, 200$. For each initial set-up, we compute particle trajectories for an integration length of $T = \pm 100$ (forward time to get repelling material lines (blue), backward time for attracting material lines (red)). For the data at Kubo number $K = 1.25$, we use the same set-up but with initial particles seeded on a $[5,\ 15]^2$ grid of meshsize 0.04 and halving the integration time span to $T = \pm 50$ (which is due to the much faster dynamics). For the static case ($K = \infty$) one frame of the data set for $K = 5$ is used and treated as autonomous data. Here, initial particles are seeded on the same grid as for $K = 1.25$ but using a longer integration interval of $T = \pm 100$ again.

A.2 Plasma data

The data is provided on a periodic $[0,\ 150] \times [0,\ 125.66]$ grid with meshsizes $\Delta x = 1.5625$ and $\Delta y = 0.9817$. The time resolution is $\Delta\tau = 0.5$ on 199 data frames. For our computations the initial particles are seeded on a $[30,\ 50] \times [20,\ 40]$ grid with meshsize 0.08 at initial times $n\Delta\hat{\tau}$, $n = 0, \ldots, 300$ and $\Delta\hat{\tau} = 0.1$ (resolution of movie). For the Runge–Kutta scheme, we choose a step size $h = 0.02$ and integrate for $T = \pm 2$.

A.3 Visualization and animations

All computations are carried out in MATLAB. For the visualization of the results, we use the patch plot command in MATLAB where the patches are colored according the FTLE values of the respective grid points (each initial point is identified with a patch). For better differentiation, we have applied a special coloring scheme that allows us to show dominant structures for the backward FTLE field (red) and the forward FTLE field (blue) at the same time.

To keep the file sizes small, some of the animations will contain less frames than described above. High resolution movies are available from the authors upon request.

References

[1] Goldston R J and Rutherford P H 1995 *Introduction to Plasma Physics* (Bristol: Institute of Physics Publishing)
[2] Naulin V, Nielsen A H and Rasmussen J J 1999 *Phys. Plasmas* **6** 4575
[3] Basu R, Jessen T, Naulin V and Rasmussen J J 2003 *Phys. Plasmas* **10** 2696
[4] Balescu R 2005 *Aspects of Anomalous Transport in Plasmas* (Bristol: Institute of Physics Publishing)

[5] Hauff T and Jenko F 2006 *Phys. Plasmas* **13** 102309
[6] Kubo R 1963 *J. Math. Phys.* **4** 174
[7] Hauff T and Jenko F 2007 *Phys. Plasmas* **14** 092301
[8] Haller G 2000 *Chaos* **10** 99
[9] Haller G and Yuan G 2000 *Physica* D **147** 352
[10] Haller G 2001 *Physica* D **149** 248
[11] Shadden S C, Lekien F and Marsden J E 2005 *Physica* D **212** 271
[12] Jenko F, Dorland W, Kotschenreuther M and Rogers B N 2000 *Phys. Plasmas* **7** 1904
[13] Dannert T and Jenko F 2005 *Phys. Plasmas* **12** 072309
[14] Vesely F J 1994 *Computational Physics* (New York: Plenum)
[15] Vlad M, Spineanu F, Misguich J H, Reuss J D, Balescu R, Itoh K and Itoh S I 2004 *Plasma Phys. Control. Fusion* **46** 1051
[16] Gruzinov A V, Isichenko M B and Kalda Y L 1990 *Sov. Phys.—JETP* **70** 263
[17] Isichenko M B 1992 *Rev. Mod. Phys.* **64** 961
[18] Reuss J H and Misguich J D 1996 *Phys. Rev.* E **54** 1857
[19] Reuss J D, Vlad M and Misguich J H 1998 *Phys. Lett.* A **241** 94
[20] Poje A C, Haller G and Mezić I 1999 *Phys. Fluids* **11** 2963
[21] Haller G 2002 *Phys. Fluids* **14** 1851
[22] Mancho A M, Small D, Wiggins S and Ide K 2003 *Physica* D **182** 188
[23] Padberg K 2005 Numerical analysis of transport in dynamical systems *PhD Thesis* University of Paderborn
[24] Miller P D, Jones C K R T, Rogerson A M and Pratt L J 1997 *Physica* D **110** 105
[25] Jones C K R T and Winkler S 2002 *Handbook of Dynamical Systems II: Towards Applications* ed B Fiedler, G Iooss and N Kopell (Singapore: World Scientific) p 55
[26] Koh T-Y and Legras B 2002 *Chaos* **12** 382
[27] Lekien F, Coulliette C, Mariano A J, Ryan E H, Shay L K, Haller G and Marsden J E 2005 *Physica* D **210** 1
[28] Wiggins S 2005 *Annu. Rev. Fluid Mech.* **37** 295
[29] Shadden S C, Dabiri J O and Marsden J E 2006 *Phys. Fluids* **18** 047105
[30] Mathur M, Haller G, Peacock T, Ruppert-Felsot J E and Swinney H L 2007 *Phys. Rev. Lett.* **98** 144502
[31] Guckenheimer J and Holmes P 1983 *Nonlinear Oscillations, Dynamical Systems, and Bifurcations of Vector Fields* (New York: Springer)
[32] Rom-Kedar V and Wiggins S 1990 *Arch. Ration. Mech. Anal.* **109** 239
[33] Boffetta G, Lacorata G, Redaelli G and Vulpiani A 2001 *Physica* D **159** 58
[34] von Hardenberg J, Fraedrich K, Lunkeit F and Provenzale A 2000 *Chaos* **10** 122
[35] Frieman E A and Chen L 1982 *Phys. Fluids* **25** 502
[36] Hahm T S, Lee W W and Brizard A 1988 *Phys. Fluids* **31** 1940
[37] Brizard A 1989 *J. Plasma Phys.* **41** 541
[38] Liewer P C 1985 *Nucl. Fusion* **25** 543
[39] Froyland G, Padberg K, England M H and Treguier A M 2007 *Phys. Rev. Lett.* **98** 224503